EVALUATION OF EROSION RESISTANCE OF ADDITIVE 3D PRINTED MATERIALS UNDER CONTINUOUS AND PULSATING WATER JET EXPOSURE

JANA PETRU[1], RADIM SKOREPA[1], AKASH NAG[1], GABRIEL STOLARIK[2], SERGEJ HLOCH[3]

[1]Faculty of Mechanical Engineering, VSB - Technical University of Ostrava, Ostrava, Czech Republic

[2]Faculty of Manufacturing Technologies, Technical University of Kosice with a seat in Presov, Slovak Republic

[3]Institute of Geonics, The Czech Academy of Sciences, Ostrava, Czech Republic

DOI: 10.17973/MMSJ.2025_03_2025006

e-mail to corresponding author: jana.petru@vsb.cz

Additively manufactured/printed represent a high potential for their use in various branches of technical practice. However, their applicability requires knowledge of the maximum application limits, or the intensity of their damage due to external factors. This article investigates the testing of 3D printed materials produced via Selective Laser Melting (SLM) treated by an ultrasound excited pulsating water jet (PWJ). The study focuses on two frequencies, 20 kHz and 40 kHz, applied to AISI 316L stainless steel and AlSiMg10 aluminium alloy. The time exposure ranged from 0.5 seconds to 10 seconds, with increments of 0.5 seconds. The water jet was pressurized to 40 MPa using a high-pressure pump, and a nozzle with a diameter of 0.4 mm was employed. The primary objective of this research is to explore the effects of ultrasonic excitation on the erosion characteristics and surface integrity of SLM-manufactured materials. The results showed that both the time exposure and the modulation frequency play vital role in determining erosion depth. Also, the surface conditions of the material are significant in erosion magnitude. Therefore, by systematically varying the exposure time and frequency, the study provided a comprehensive understanding of how these parameters influence the erosion evolution and performance of the tested materials.

KEYWORDS

ultrasonic pulsating water jet, erosion of additively manufactured, droplet erosion resistance, erosion depth, Selective Laser Melting

1 INTRODUCTION

Additive manufacturing can create materials customized to specific requirements. Among these different methods of additive manufacturing, selective laser melting (SLM) is the most widely used technology for processing various metallic materials (Srivastava et al., 2024). Due to the unique microstructures formed by the intricate nature of SLM, materials produced through SLM exhibit significantly different properties compared to their conventionally manufactured counterparts When porosity in 3D-printed components is ensured, SLM-produced materials exhibit significantly greater yield stress, ultimate tensile strength, and hardness compared to their traditionally manufactured counterparts Besides being tested for various desired parameters, these materials must also withstand repeated external loads, such as water droplets in certain applications. Historically, water droplet erosion was primarily observed on steam turbine blades (Medraj, 2017). These blades were struck by condensed water from the steam (Medraj, 2017), (Stanisa & Ivusic, 1995), gradually losing their aerodynamic shape, which led to a decline in performance and efficiency (Cook, 1928). To determine erosion resistance and development, various test devices are employed (Field, 1999). These include rotating disks (Wang et al., 2022), whirling wheels, and stationary sources that interrupt (Vijay et al., 1994) or modulate a continuous water flow (Szada-Borzyszkowska et al., 2024). These devices allow for the observation of erosion development, which includes the incubation, and acceleration stages (Gujba et al., 2016). The initial stages involve (Brunton & Rochester, 1979) the introduction of compressive stresses without any observed mass removal, while the advanced phases are characterized by the loss of mass from the base material (Adler, 1979; Hancox & Brunton, 1966). The time scale depends on several factors, such as the impact velocity of the drop, its density, temperature, and Weber number (Ahmad et al., 2018). From a material perspective, key parameters include hardness (Poloprudsky et al., 2021), heat treatment, grain size (Lehocka et al., 2017), and production method (N. Fujisawa et al., 2015). Since additive manufacturing differs from conventional methods like casting and rolling, it results in the formation of specific microstructures with so-called melt pools (Lin et al., 2024) and cellular dislocation structure (Šmíd et al., 2023). Current research primarily focuses on conventional materials and methods, leaving a gap in understanding how additively manufactured materials, with their unique properties, respond to erosion. Factors such as frequency and drop density are known to influence erosion, but their effects on additively manufactured materials need further investigation. Therefore, there is a need for targeted research to evaluate the erosion resistance of additively manufactured materials such as AISI 316 L and aluminium alloy (Poloprudsky et al., 2022), considering their unique production methods and properties using ultrasonic pulsating water jet (Foldyna et al., 2006; Nastic et al., 2023).

Therefore, in the present study, PWJ as a droplet generator is used for determining the erosion resistance of SLM printed AISI 316L and AlSi10Mg material in terms of erosion depth using two water cluster volumes V = 1.6 mm^3 and 0.82 mm^3 obtained by using modulation frequency f = 20 kHz and 40 kHz. The water clusters velocities were kept as v = 260 m/s controlled by supply pressure p = 40 MPa and to observe the time dependence of the erosion, the time exposure was varied from 0.5 s to 10 s in increments of 0.5 s. The surface erosion was quantified by erosion depth and qualitatively observed by surface topography images of the eroded craters after the PWJ interaction.

2 MATERIALS AND METHODS

2.1 *Materials*

The present study used additively manufactured aluminium alloy (AlSi10Mg) and austenitic stainless steel (AISI 316L) as workpiece samples. The materials were additively manufactured using SLM technology. Renishaw AM 500 flex was used to print both materials. The materials were printed using standard technological parameters provided by the OEM, shown in Tab. 1. The sample dimensions were 150x40x10 mm for both tested materials. The samples were cut from the build plate using Wire EDM machining for precise and accurate

cutting. The manufactured sample surface roughness was measured to be Ra 7.7µm, Rz 78.81 for AISI 316L and Ra 8.4µm, Rz 74.13 for AlSi10Mg, which is typical for additively manufactured samples using SLM technology.

Printing parameter	AlSi10Mg	AISI 316L
Laser Power (W)	500	200
Scan speed (mm/s)	1875	650
Layer thickness (mm)	0.06	0.05
Hatch distance (mm)	0.09	0.11
Laser spot size (mm)	0.075	0.075
Scanning strategy	Stripes	Stripes
Preheat (°C)	170°	

Table 1. Printing parameters used for printing AlSi10Mg and AISI 316L

2.2 *Experimental method*

The experiment focuses on the erosion testing of austenitic stainless steel AISI 316L and aluminium alloy AlSi10Mg using hybrid technology combining ultrasound and water jet, well known as ultrasonic pulsating water jet (Vijay et al., 1993) patented at the Institute of Geonics by (Foldyna & Svehla, 2008, 2010). The technological equipment produces pressure fluctuations in the acoustic chamber (Foldyna et al., 2004, 2006), by a method of stimulation of the piezoceramic materials (Nag & Hloch, 2025). In the set-up of this experiment, stimulation frequencies of 20 and 40 kHz were used as a basis for comparison of the different erosion states produced on the applied materials. These frequencies generated water cluster volumes V = 1.6 mm³ and 0.82 mm³ for 20 and 40 kHz, respectively.

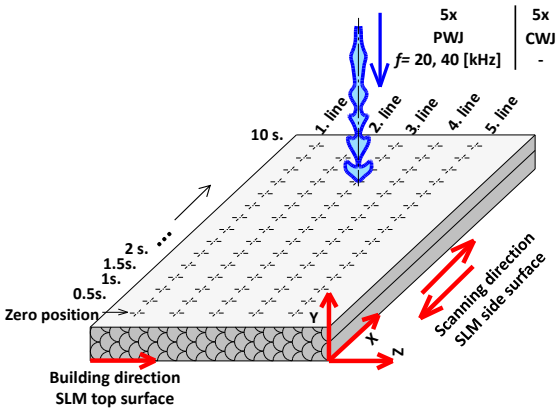

Figure 1. Schematic representation of the experimental setup.

As a result, shortly after exiting the nozzle, the water jet breaks into clusters of water droplets that impact the material. A crucial step in the process is optimizing the pulsating water jet technology to achieve maximum erosion efficiency for flow rate determined by supply pressure p = 40 MPa and nozzle diameter d = 0.4 mm (Nag et al., 2022). The resonance frequency and impedance range for the pulsating water jet technology are adjusted by varying the length of the acoustic chamber (Nag, et al., 2021). Based on previous experiments, it was determined that for an applied pressure of p = 40 MPa, the optimal length of the acoustic chamber (Nag et al., 2019) is lc = 10 mm. Further, an optimal distance between the nozzle and the surface of the tested material using a stair trajectory was set to be = 19 mm (Hloch et al., 2020). The experimental setup for the present study is shown in Fig. 1. The experimental conditions of the study are tabulated in Tab.2. For each technological setting, five repetitions were done to be statistically accurate. For comparing the efficiency of the PWJ over continuous water jet (CWJ), the same experiments were repeated for both materials, keeping the hydraulic and technological parameters the same as PWJ.

Technological parameter	Value		
Supply pressure p (MPa)	40		
Modulation frequency f (kHz)	20	40	CWJ
Water cluster volumes (mm³)	1.6	0.82	--
Acoustic chamber length lc (mm)	10		
Nozzle diameter d (mm)	0.4		
Standoff distance z (mm)	19		
Time exposure (s)	0.5 - 10		

Table 2. Technological parameters of PWJ used for the experiments.

2.3 *Measurement*

The erosion resistance of the printed materials was evaluated based on their erosion depth when subjected to the PWJ. To evaluate the erosion depth, the entire sample after the exposure to PWJ as per technological parameters mentioned in Tab. 2 was scanned using an Alicona G5 Infinite optical microscope (See Fig. 2). The 5x objective lens with a field view area of 7.95 mm² was used to scan the impacted surface of the materials. With this objective, a vertical resolution of 410 nm was obtained, providing a precise measurement of the different structures generated due to the interaction of the PWJ with the samples. After scanning, the scanned data was transferred to MountainsMap software to analyze or evaluate the depth of the erosion craters generated by the PWJ. The deepest point of each crater was used to plot the erosion trend with different time exposures. During the evaluation, it was found that CWJ for the given conditions didn't create any measurable erosion traces or craters on both the materials under investigation. This significant difference in erosion between the PWJ and CWJ is attributed to the utilization of impact pressure for PWJ and stagnation pressure for CWJ. Therefore, CWJ erosion craters were not evaluated or analyzed further.

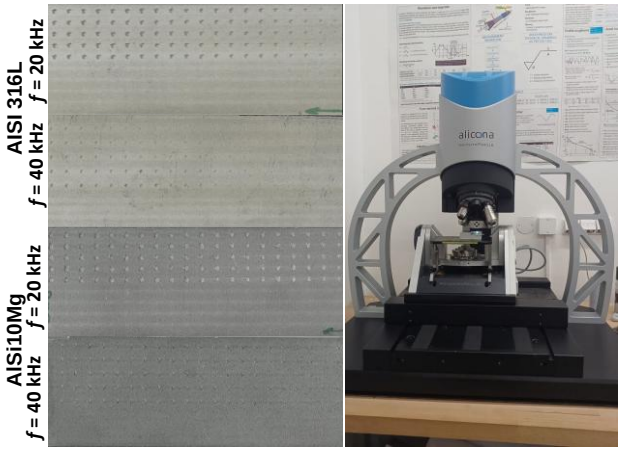

Figure 2. Pictorial view of SLM printed AISI 316L and AlSi10Mg samples after the experiment using Alicona G5 optical microscope

3 RESULTS AND DISCUSSION

The results illustrate the time-dependent erosion evolution in 3D printed materials. The findings highlight the impact of multiple droplet impingements on SLM-manufactured materials under various kinematic parameters of the water droplets. This

study examines how frequency and droplet size influence erosion evolution using a more advanced methodology compared to the approach used in (Mednikov et al., 2019). In this study, the capability of ultrasound-excited jets to focus individual pulses on a specific location was utilized (Foldyna et al., 2004). This approach allowed us to observe the development at that location and correlate the erosion progression to specific areas presented in (Hloch et al., 2024; Poloprudsky et al., 2024). Fig. 3a illustrates the erosion resistance of SLM-printed AISI 316L, assessed by erosion depth over increasing exposure times. Both experimental conditions (frequencies of 20 kHz and 40 kHz) show an increasing trend in erosion depth with longer exposure. At 20 kHz and 0.5 seconds of exposure, no visible erosion crater was detected, indicating the incubation stage of erosion. During this stage, the repetitive action of the jet cannot induce the failure that surpasses the material's ultimate fatigue strength, i.e., no visible fractures or erosion occurs. However, when the exposure time increases to 1 second (i.e., 20,000 impacts), material erosion becomes apparent, with a depth of 34 ± 8 µm. The repetitive impingements generate compressive stress, and deforms the surface, generating micro dimples and cracks. These surface defects under further impingement propagate across the impact epicentre and coalesce to form deeper and wider craters (Luiset et al., 2013). With further increase in the time exposure, the erosion depth increases. The erosion depth increases from h = 34 ±8 µm to 196 ±18 µm for the increase in exposure time t = 1 to 10 s. The variability in the measurements observed by the error bars can be attributed to the local surface and material properties of the sample and improper transmission of the ultrasonic signals (Stolarik et al., 2023). Moreover, the rate of increase in the erosion depth is slightly lower for the higher exposure time range t = 7 to 10 s compared to t = 0.5 to 7 s. This can be attributed to the resistance of the stagnant water layer already present towards the incoming jet when interacting with the material. Also, the surface roughness formed by the initial impacts breaks the subsequent jet, resulting in energy loss and lower penetration into the material to achieve higher depth. Therefore, for t = 10 s, the erosion depth slightly decreases to 196 ±18 µm compared to 201 ±22 µm for t = 9.5 s. A similar trend for both frequencies was observed in (Nag, Hvizdos, et al., 2021). For a modulation frequency of 40 kHz, the erosion depth followed a similar trend to that observed at 20 kHz. However, the incubation phase for material exposed to 20 kHz lasted for 0.5 s, whereas for 40 kHz, it extended to 5 s. This prolongation is due to the smaller volume of individual clusters impacting the surface at 40 kHz compared to 20 kHz. The theoretical volumes of each water cluster are 1.64 mm³ for 20 kHz and 0.82 mm³ for 40 kHz. This difference in cluster volume affects the mass and kinetic energy of the jet. Consequently, at 40 kHz, the lower impact energy during shorter exposure times allows the material to retain its integrity without visible erosion. However, with longer exposure times (5 s), the cumulative stress induces material failure, resulting in visible and measurable erosion craters. The erosion depth increases from 15 ± 7 µm to 49 ± 25 µm as exposure time increases from 5 to 10 s. The erosion depth increase at 20 kHz is nearly 368% higher than at 40 kHz for 9.5 seconds, highlighting the significance of water cluster volume in determining the erosion efficiency of PWJ. Variability in erosion depth for the same exposure time is also observed due to the same reasons mentioned for 20 kHz. Therefore, it can be concluded that SLM-printed AISI 316L exhibits erosion resistance to water droplets with an impact velocity of 260 m/s for exposure times of 0.5 and 5 seconds, with droplet volumes of 1.64 mm³ and 0.82 mm³ at frequencies of 20 and 40 kHz, respectively. This observation aids in effective planning for preventive maintenance to avoid material failure during operational conditions.

The erosion resistance trend of the SLM printed AlSi10Mg material is represented in terms of erosion depth with increasing time exposure, as shown in Fig. 3b. The trend of erosion depth is similar to that of AISI 316L with increasing time exposure. However, for AlSi10Mg samples, the material erosion was observed from starting of the exposure time, i.e., t = 0.5 s for both the modulation frequencies. Therefore, no incubation phase of the erosion was detected for this material. This phenomenon can be attributed to the lower mechanical properties of AlSi10Mg (R_m = 352 MPa) as compared to AISI 316L (R_m = 540 MPa) (Concli et al., 2023) which leads to lesser resistance towards the PWJ and shows material erosion even with lower time exposure. The erosion depth increased from h = 223 ±32 µm to 441 ±46 µm for an increase in the exposure time t = 0.5 to 10 s. This increasing trend is more evident till time exposure t = 7.5 s, after which the erosion depth decreases even with increasing time exposure. This is due to the same reason mentioned for the decrease in the erosion magnitude of the AISI 316L sample, i.e., resistance offered by the stagnant water layer in the generated crater created by initial water clusters leading to reduced interaction of the subsequent water clusters with the material. Also, due to the formation of peaks and valleys, the proper impact of the water clusters is affected, leading to reduced stress induction into the material and lower erosion depth. However, for the AlSi10Mg sample, the erosion depth trend for lower time exposures is also not very steady and uniform and shows a stochastic trend. This can be due to the roughness of the impact surface, which has a significant influence on the erosion characteristic of the PWJ. Also, it can be attributed to the manufacturing defect involving local defects during the printing of the material. Therefore, proper testing of the additively printed material along with surface preparation is an important step for future experiments.

For f = 40 kHz, the erosion magnitude measured in terms of erosion depth shows overall lower values for almost the entire time exposure range tested in the present study. This is similar to the trend observed for AISI 316L material exposure to f = 40 kHz, which is attributable to lower water droplet volume impacting the material. However, the difference in the magnitude of erosion depth between f = 20 and 40 kHz for AISI 316L is much larger and more evident than that observed for AlSi10Mg. This can be attributed to the mechanical properties and the impact pressure induced by the PWJ. The ultimate strength of the aluminium alloy is nearly 35% lower than that of stainless steel, making it less erosion resistant even with a jet with lower kinetic energy due to a smaller water cluster volume. The erosion depth changes from h = 158 ±20 µm to 488 ±17 µm for exposure time increasing from 0.5 to 10 s. For same technological conditions such as f = 20 kHz and t = 9.5 s, the erosion depth for AlSi10Mg is 152% more than AISI 316L showcasing the greater erosion resistance of the steel towards hydrodynamic loads. It is directly connected to the better mechanical properties of the AISI 316L material as compared with AlSi10Mg.

The erosion evolution can be interpreted by the following regression equations (see (1) to (4)). The equation (1) describes how the depth created by erosion at a frequency of 20 kHz changes over time, with a very high degree of accuracy. The natural logarithm of a time exposure at the beginning of erosion increases rapidly. Therefore, the depth created at the frequency of f = 20 kHz increases quickly at the beginning of the erosion process. This phenomenon agrees with the

conventionally accepted theory of the acceleration erosion stage (Ahmad et al., 2018) or accumulation erosion stage (K. Fujisawa, 2023). As time increases, the natural logarithm function grows more slowly, which means the rate of increase in erosion depth also slows down which corresponds to the attenuation erosion stage. At this stage, the depth increases very slowly, exhibiting asymptotic behavior as it approaches its limit. On the other hand, the coefficient for f = 40 kHz is 10.83 (2), while for 20 kHz it is 83.45. This suggests that the depth created at 20 kHz increases much more rapidly compared to 40 kHz (Figure 4). From equations (1,2) and the plot (Fig. 3a) for the AISI 316L steel, the depth created at f = 20 kHz increases much more rapidly compared to f = 40 kHz which corresponds to the higher coefficient. Even though the frequency has doubled, resulting in twice the bulk density of droplets, these droplets do not possess the same necessary erosion energy. The response of aluminium alloy to the ultrasonic pulsating water jet is characterized by equations (3,4). The higher coefficients for AlSi10Mg alloy compared to the AISI316L material suggest that AlSi10Mg alloy erodes more effectively under the same PWJ conditions. Also, in this case, the erosion process is more effective at f = 20 kHz compared to f = 40 kHz, as indicated by the higher coefficient (4).

$$316L_{h20} = 83.45 \cdot \ln(t + 0.378)\ ;\ R^2 = 0.958 \quad (1)$$

$$316L_{h40} = 21.49 \cdot \ln(t - 3.91)\ ;\ R^2 = 0.788 \quad (2)$$

$$AlSi10Mg_{h20} = 212.38 \cdot \ln(t + 3.254)\ ;\ R^2 = 0.749 \quad (3)$$

$$AlSi10Mg_{h40} = 170.96 \cdot \ln(t + 2.357)\ ;\ R^2 = 0.889 \quad (4)$$

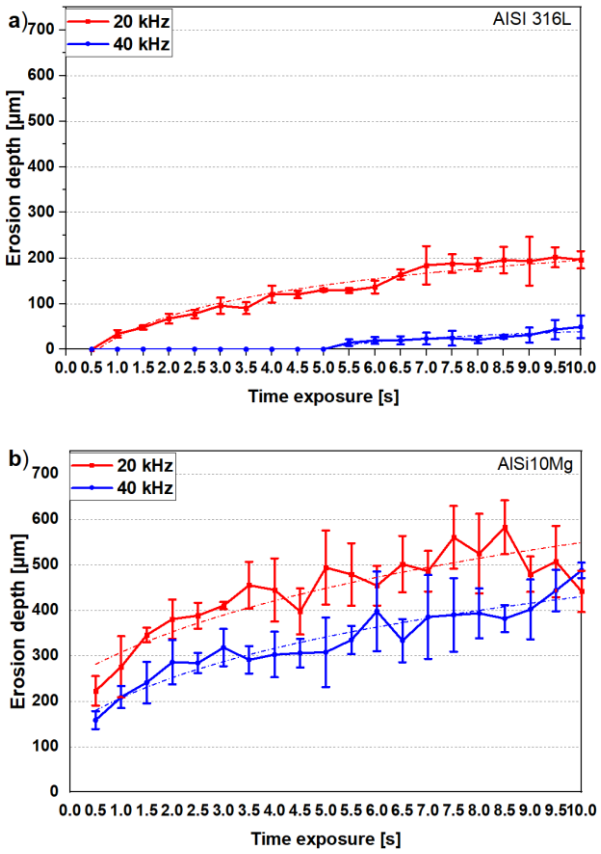

Figure 3. Graphical depiction of erosion depth over time for modulation frequencies of 20 kHz and 40 kHz for a) SLM printed AISI 316L, and b) for SLM printed AlSi10Mg including all relevant parameters within the graph

The characterization of erosion stages was performed by the method of optical analysis and 3D reconstruction of individual erosion craters. Due to the higher number of experimental conditions on the samples and the repeatability of the process, representative areas of erosion craters were selected, which are discussed further. To capture the overview analysis, 3 representative time exposures, t = 0.5, 5 and 10 s were selected, which were compared on each material with respect to the change in the modulation frequency/volume of water clusters. From the optical analysis presented in Fig. 4a, it is possible to confirm that the initial time exposure for the SLM printed AISI 316L material did not cause significant erosion damage or any loss of the material. However, it is possible to observe shadow areas, which may mean only surface cleaning without significant material removal. The overall view of the material shows a diverse coloration of grey and black areas, which indicates its inhomogeneity. With increasing time exposure to 5 and 10 s, there is visible removal and loss of material. The bottom of the erosion craters shows a solid shape with a certain stochastic structure of the roughened area.

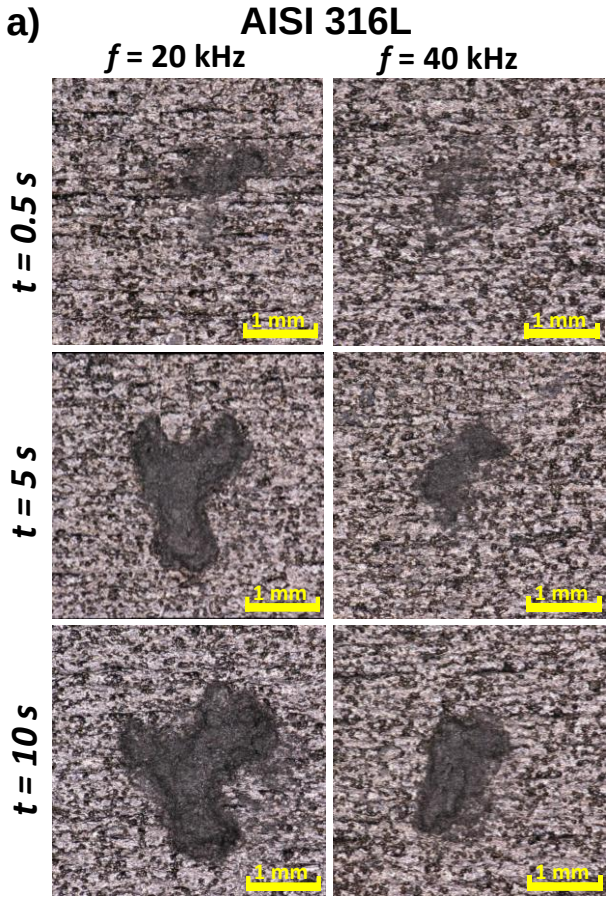

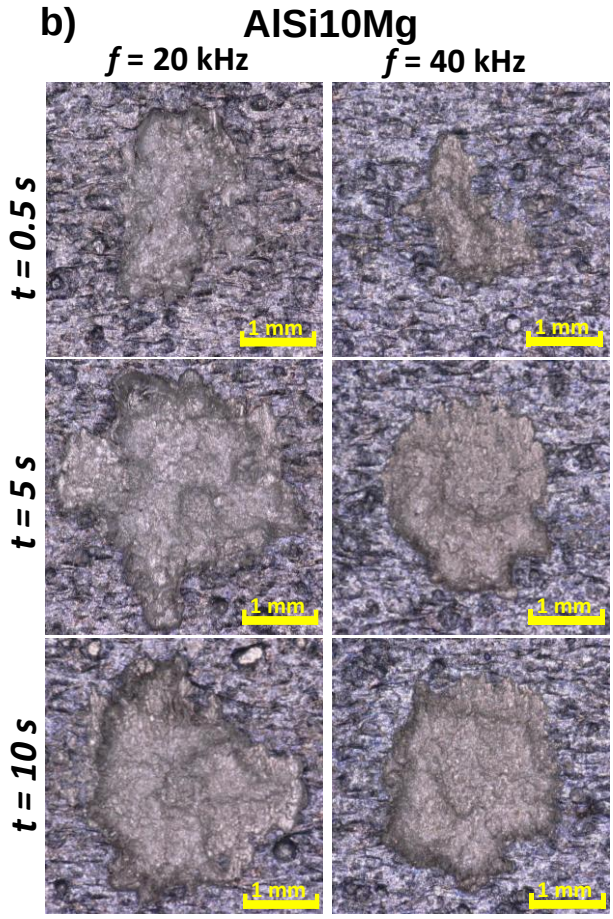

Figure 4. Erosion patterns generated by PWJ with modulation frequencies of 20 kHz and 40 kHz on SLM printed a) AISI 316L and b) AlSi10Mg Aluminium Alloy observed using optical microscope.

Erosion patterns for AlSi10Mg (Fig. 4b) confirmed the absence of an incubation phase of erosion. Even at the lowest time exposure of 0.5 s, material was removed at both 20 and 40 kHz. With increasing time exposure, this erosion increased significantly, especially when looking at the diameters of the erosion craters. The bottom of the craters has a significantly inhomogeneous shape and is composed of distinct peaks and valleys. However, these do not show any sharp edge that could locally weaken the bottom of the erosion pit. From the optical analysis of the surface, it can be further seen that the shape of craters has an approximately circular shape, except for the frequency of 40 kHz at time exposure 0.5 s. In this case, smaller volumes of water clusters caused only minor damage to the material, which can be classified as the initial phases of removal. The lower time exposure did not allow this erosion to spread into a solid circular shape, so the erosion was most significant only at weakened points of the material. This caused its inhomogeneity, as also observed in AISI 316L.

The 3D surface topography of erosion craters for AISI 316L confirmed that deeper erosion craters are recorded at a modulation frequency of 20 kHz compared to 40 kHz (Fig. 5a). These craters can be compared to a Y shape. Such a crater shape could be caused by water seeking the easiest path through the material, and thus areas where material defects or inhomogeneities are found are eroded first. Moreover, it can also be caused by the inadequate perpendicular angle of the impact of water clusters on the material, leading to greater erosion on one side compared to the other. Therefore, potential material defects had the opportunity to expand, while the surrounding solid material was able to better resist erosion. In this way, inhomogeneous erosion shapes could be created.

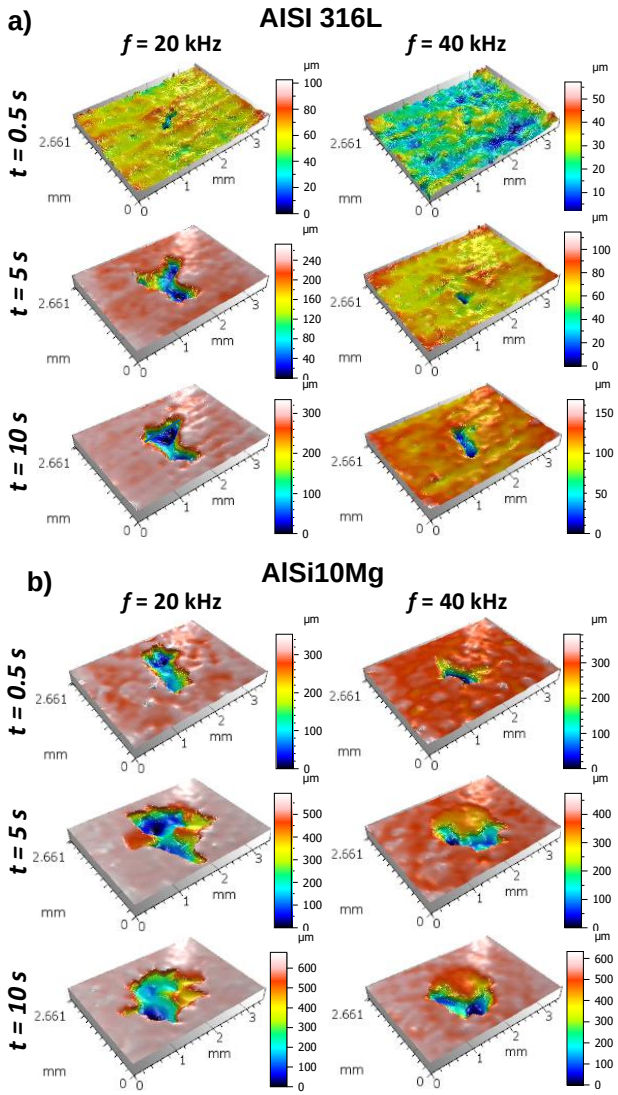

Figure 5. 3D surface topography of the craters generated by PWJ with modulation frequencies of 20 kHz and 40 kHz on SLM printed a) AISI 316L and b) AlSi10 Mg aluminium alloy

For AlSi10Mg, the 3D surface topography of erosion craters showed that the apparently round shape from optical analysis is distorted from the perspective of material depth (Fig. 5b). In this view, it can be seen that the erosion pit has a crescent shape at 40 kHz, which is deeper on one side. This can be explained by the fact that the material was initially removed in an irregular shape (observed at 0.5 s), where however, increasing time exposure causes the erosion to spread, and the removal of surface layers of material also in the area that originally resisted erosion. However, this trend is observed only at 40 kHz, where none of the aforementioned phenomena are visible in comparison to 20 kHz. Therefore, it is clear that larger volumes of water clusters cause sufficient loading of the material to ensure that the target material is removed more evenly.

These optical analyses thus show that the degree of damage to the SLM printed surfaces depends mainly on the mechanical properties of the material. This affects the shape of the erosion crater, which in the case of AISI 316L showed a solid shape, compared to AlSi10Mg, where the bottom was formed by peaks and valleys. Furthermore, the volume of water clusters changes the intensity of damage, where the AlSi10Mg material

is removed inhomogeneously in the form of a crescent shape with smaller drops (40 kHz). In contrast, larger drops result in a more uniform distribution of loading forces, resulting in its removal in a circular shape.

4 CONCLUSIONS

The present study evaluates the erosion resistance of additively printed AISI 316L and AlSi10Mg samples exposed to hydrodynamic loading of water clusters. Ultrasonic PWJ was used as a droplet generator with modulation of frequencies f = 20 and 40 kHz, producing water cluster volume of V = 1.6 mm^3 and 0.81 mm^3, respectively along with variations in time exposure from 0.5 to 10 seconds in increments of 0.5 seconds. The main conclusive results of the study are as follows:

- With an increase in time exposure (t = 0.5 to 10 s), the erosion depth increases for all tested conditions due to the higher number of repetitive impacts (10,000 to 200,000 impacts and 20,000 to 400,000 impacts for 20 and 40 kHz, respectively), resulting in larger compressive stress at the impact site.
- The erosion depth also depends on the modulation frequency, which determines the volume of individual water clusters (V = 1.6 mm^3 and 0.81 mm^3 for f = 20 and 40 kHz, respectively) and, consequently, the kinetic energy of the clusters impacting the material.
- AISI 316L exhibited a five times longer incubation period (t = 5 s) compared to AlSi10Mg (t = 1 s) under the same technological conditions, attributed to the mechanical and surface properties of the samples
- Erosion depth at 20 kHz increases rapidly initially, then slows down over time, aligning with accepted erosion theories and exhibiting asymptotic behavior as it approaches its limit.
- Erosion depth at 20 kHz increases much more rapidly than at 40 kHz, despite the higher droplet density at 40 kHz (40,000 impacts) than 20 kHz (20,000 impacts), due to the higher erosion energy at 20 kHz linked to water cluster volume (V = 1.6 mm^3 and 0.81 mm^3 for f = 20 and 40 kHz, respectively).
- AlSi10Mg erodes more effectively than AISI 316L under the same conditions, with the erosion process being more effective at 20 kHz compared to 40 kHz.
- Surface topography images revealed the stochastic geometry of the craters generated after the jet impacts.

This study presents the utilisation of PWJ as a droplet generator capable of producing droplets under various hydraulic conditions. The generated droplets enable the accelerated assessment of erosion resistance in materials subjected to hydrodynamic flow conditions. Future studies can further investigate the influence of additional technological input parameters on the erosion resistance of newly developed materials.

ACKNOWLEDGMENTS

The financial support received from the Czech Science Foundation, project GAČR 23–05372S, is gratefully acknowledged.

REFERENCES

[Adler 1979] Adler, W. F. The mechanics of liquid impact. Academic Press, Treatise on Materials Science and Technology, 1979, 16, 127–183.

[Ahmad 2018] Ahmad, M., Schatz, M., & Casey, M. V. An empirical approach to predict droplet impact erosion in low-pressure stages of steam turbines. Wear, 2018, 402–403, 57–63.

[Brunton 1979] Brunton, J. H., & Rochester, M. C. Erosion of solid surfaces by the impact of liquid drops. Academic Press, Treatise on Materials Science and Technology, 1979, 16, 185–248.

[Concli 2023] Concli, F., Gerosa, R., Panzeri, D., & Fraccaroli, L. High and low cycle fatigue properties of selective laser melted AISI 316L and AlSi10Mg. International Journal of Fatigue, 2023, 177, 107931.

[Cook 1928] Cook, S. S. Erosion by water-hammer. Proceedings of the Royal Society of London. Series A, Containing Papers of a Mathematical and Physical Character, 1928, 119(783), 481–488.

[Field 1999] Field, J. E. ELSI conference: Invited lecture liquid impact: Theory, experiment, applications. Wear, 1999, 233–235, 1–12.

[Foldyna 2006] Foldyna, J., Sitek, L., & Haban, V. (2006). Acoustic wave propagation in high-pressure system. Ultrasonics, 2006, 44.

[Foldyna 2004] Foldyna, J., Sitek, L., Svehla, B., & Svehla, S. Utilization of ultrasound to enhance high-speed water jet effects. Ultrasonics Sonochemistry, 2004, 11(3–4), 131–137.

[Foldyna 2008] Foldyna, J., & Svehla, B. Patent Application Publication (10) Pub . No .: US 2008 / 0135638 A1. In Patent Application Publication (10) Pub . No .: US 2008 / 0135638 A1, 2008.

[Foldyna 2010] Foldyna, J., & Svehla, B. Method of generation of pressure pulsations and apparatus for implementation of this method. Google Patents, 2010.

[Fujisawa 2023] Fujisawa, K. On erosion transition from the incubation stage to the accumulation stage in liquid impingement erosion. Wear, 2023, 528–529.

[Fujisawa 2015] Fujisawa, N., Yamagata, T., Takano, S., Saito, K., Morita, R., Fujiwara, K., & Inada, F. The influence of material hardness on liquid droplet impingement erosion. Nuclear Engineering and Design, 2015.

[Gujba 2016] Gujba, A. K., Hackel, L., Kevorkov, D., & Medraj, M. Water droplet erosion behaviour of Ti-6Al-4V and mechanisms of material damage at the early and advanced stages. Wear, 2016, 358–359, 109–122.

[Hancox 1966] Hancox, N. L., & Brunton, J. H. The Erosion of Solids by the Repeated Impact of Liquid Drops. Philosophical Transactions of the Royal Society of London. Series A, Mathematical and Physical Science, 1966.

[Hloch 2024] Hloch, S., Poloprudsky, J., Siska, F., Babinsky, T., Nag, A., Chlupová, A., & Kruml, T. (2024). Erosion development in AISI 316L stainless steel under pulsating water jet treatment. Engineering Science and Technology, an International Journal, 2024, 50.

[Hloch 2020] Hloch, S., Srivastava, M., Nag, A., Muller, M., Hromasova, M., Svobodova, J., Kruml, T., & Chlupova, A. Effect of pressure of pulsating water jet moving along stair trajectory on erosion depth, surface morphology and microhardness. Wear, 2020, 452–453.

[Lehocka 2017] Lehocka, D., Klichova, D., Foldyna, J., Hloch, S., Hvizdos, P., Fides, M., & Botko, F. Comparison of the influence of acoustically enhanced pulsating water jet on selected surface integrity characteristics of CW004A copper and CW614N brass. Measurement: Journal of the International Measurement Confederation, 2017, 110.

[Lin 2024] Lin, Y.-T., Tsai, M.-Y., Yen, S.-Y., Lung, G.-H., Yei, J.-T., Hsu, K.-J., & Chen, K.-J. Comparing the Performance of Rolled Steel and 3D-Printed 316L Stainless Steel. Micromachines, 2024, 15(3), 353.

[Luiset 2013] Luiset, B., Sanchette, F., Billard, A., & Schuster, D. Mechanisms of stainless steels erosion by water droplets. Wear, 2013, 303(1–2), 459–464.

[Srivastava 2024] Srivastava, M., Jayakumar, V., Udayan, Y., Sathishkumar, M., Muthu, S. M., Gautam, P., & Nag, A. Additive manufacturing of Titanium alloy for aerospace applications: Insights into the process, microstructure, and mechanical properties. Applied Materials Today, 2024, 41, 102481.

[Mednikov 2019] Mednikov, A. F., Tkhabisimov, A. B., Zilova, O. S., Burmistrov, A. A., & Sidorov, S. V. The results of water droplet erosion tests of ion-plasma coatings formed on titanium Ti-6Al-4V alloy samples manufactured by using 3D-printing and traditional technological process. IOP Conference Series: Materials Science and Engineering, 2019, 537(2), 022066.

[Medraj 2017] Medraj, H. S. K. and D. K. and A. U. and M. Water droplet erosion of stainless steel steam turbine blades. Materials Research Express, 2017.

[Nag 2025] Nag, A., & Hloch, S. Disintegration of Bone Cement Using Pulsating Water Jet: A Comparative Study of Standard and Extended Nozzles. Spectrum of Mechanical Engineering and Operational Research, 2025, 2(1), 93-103.

[Nag 2022] Nag, A., Dixit, A. R., Petrů, J., Vanova, P., Konecna, K., & Hloch, S. (2022). Maximization of wear rates through effective configuration of standoff distance and hydraulic parameters in ultrasonic pulsating water jet. Facta Universitatis, Series: Mechanical Engineering, 2022.

[Nag 2019] Nag, A., Hloch, S., Cuha, D., Dixit, A. R., Tozan, H., Petrů, J., Hromasova, M., & Müller, M. Acoustic chamber length performance analysis in ultrasonic pulsating water jet erosion of ductile material. Journal of Manufacturing Processes, 2019, 47.

[Nag 2021] Nag, A., Hvizdos, P., Dixit, A. R., Petrů, J., & Hloch, S. Influence of the frequency and flow rate of a pulsating water jet on the wear damage of tantalum. Wear, 2021, 203893.

[Nag 2021] Nag, A., Stolarik, G., Svehla, B., & Hloch, S. Effect of Water Flow Rate on Operating Frequency and Power During Acoustic Chamber Tuning. Advances in Manufacturing Engineering and Materials II: Proceedings of the International Conference on Manufacturing Engineering and Materials (ICMEM 2020), 21–25 June, 2021, Nový Smokovec, Slovakia, 142–154.

[Nastic 2023] Nastic, A., Vijay, M., Tieu, A., & Jodoin, B. High speed water droplet impact erosive behavior on dry and wet pulsed waterjet treated surfaces. Physics of Fluids, 2023, 35(5).

[Poloprudsky 2021] Poloprudsky, J., Chlupova, A., Sulak, I., Kruml, T., & Hloch, S. Surface and Subsurface Analysis of Stainless Steel and Titanium Alloys Exposed to Ultrasonic Pulsating Water Jet. Materials, 2021, 14(18), 5212.

[Poloprudsky 2024] Poloprudsky, J., Gamanov, S., Chlupova, A., Klichova, D., Nag, A., Stolarik, G., & Hloch, S. Water droplet erosion assessment in the initial stages on AISI 316 L using kernel average misorientation. Tribology International, 2024, 191.

[Poloprudsky 2022] Poloprudsky, J., Nag, A., Kruml, T., & Hloch, S. Effects of liquid droplet volume and impact frequency on the integrity of Al alloy AW2014 exposed to subsonic speeds of pulsating water jets. Wear, 2022, 488–489.

[Smid 2023] Smid, M., Koutny, D., Neumannova, K., Chlup, Z., Nahlik, L., & Jambor, M. Cyclic behaviour and microstructural evolution of metastable austenitic stainless steel 304l produced by laser powder bed fusion. Additive Manufacturing, 2023, 68, 103503.

[Stanisa 1995] Stanisa, B., & Ivusic, V. Erosion behaviour and mechanisms for steam turbine rotor blades. Wear, 1995, 186–187(PART 2), 395–400.

[Stolarik 2023] Stolarik, G., Klichova, D., Poloprudsky, J., Nag, A., & Hloch, S. Assessment of surface irregularities created by controlled liquid droplet on the surface of stainless steel AISI 304L. Engineering Science and Technology, an International Journal, 2023, 47, 101558.

[Szada-Borzyszkowska 2024] Szada-Borzyszkowska, M., Kacalak, W., Banaszek, K., Pude, F., Perec, A., Wegener, K., & Królczyk, G. Assessment of the effectiveness of high-pressure water jet machining generated using self-excited pulsating heads. The International Journal of Advanced Manufacturing Technology, 2024.

[Vijay 1994] Vijay, M. M., Foldyna, J., & Remisz, J. Ultrasonic modulation of high-speed water jets. In Geomechanics 93. Proc. conference, Ostrava, 1993.

[Vijay 1993] Vijay, M. M., Remisz, J., & Shen, X. Potential of pulsed water jets for cutting and fracturing of hard rock formations. International Journal of Surface Mining, Reclamation and Environment, 1993, 7(3), 121–132.

[Wang 2022] Wang, Z., Kang, Y., Xie, F., Shi, H., Wu, N., Wang, Z., Wang, X., Hu, Y., & Li, D. (2022). Experimental investigation on the penetration characteristics of low-frequency impact of pulsed water jet. Wear, 2022, 488–489.

CONTACTS:

prof. Ing. et Ing. Mgr. Jana PETRU, Ph.D.
VSB-Technical University of Ostrava, Faculty of Mechanical Engineering
17. listopadu 2172/15, 708 00 Ostrava Poruba, Czech Republic
+420 59 732 4391, jana.petru@vsb.cz